Published in final edited form as:
Exp Eye Res. 2007 March ; 84(3): 513–528.

Transgenic overexpression of connexin50 induces cataracts

June Chung[a], **Viviana M. Berthoud**[a,*], **Layne Novak**[b], **Rebecca Zoltoski**[c], **Benjamin Heilbrunn**[a], **Peter J. Minogue**[a], **Xiaoqin Liu**[d], **Lisa Ebihara**[d], **Jer Kuszak**[b], and **Eric C. Beyer**[a]

a *Department of Pediatrics, University of Chicago, IL 60637, USA*

b *Department of Ophthalmology and Pathology, Rush University Medical Center, Chicago, IL 60612, USA*

c *Department of Basic and Health Sciences, Illinois College of Optometry, Chicago, IL 60616, USA*

d *Department of Physiology and Biophysics, Rosalind Franklin University School of Medicine, Chicago, IL 60064, USA*

Abstract

To examine the effects of increased expression of Cx50 in the mouse lens, transgenic mice were generated using a DNA construct containing the human Cx50 coding region and a C-terminal FLAG epitope driven by the chicken βB1-crystallin promoter. Expression of this protein in paired *Xenopus* oocytes induced gap junctional currents of similar magnitude to wild type human Cx50. Three lines of transgenic mice expressing the transgenic protein were analyzed. Lenses from transgenic mice were smaller than those from non-transgenic littermates, and had cataracts that were already visible at postnatal day 1. Expression of the transgene resulted in a 3- to 13-fold increase in Cx50 protein levels above those of non-transgenic animals. Light microscopy revealed alterations in epithelial cell differentiation, fiber cell structure, interactions between fiber cells and areas of liquefaction. Scanning electron microscopy showed fiber cells of varying widths with bulging areas along single fibers. Anti-Cx50 and anti-FLAG immunoreactivities were detected at appositional membranes and in intracellular vesicles in transgenic lenses. N-cadherin, Cx46, ZO-1 and aquaporin 0 localized mainly at the plasma membrane, although some N-cadherin and aquaporin 0 was associated with the intracellular vesicles. The abundance and solubility/integrity of αA-, αB-, β- and γ-crystallin were unaffected. These results demonstrate that transgenic expression of Cx50 in mice leads to cataracts associated with formation of cytoplasmic vesicles containing Cx50 and decreased or slowed epithelial differentiation without major alterations in the distribution of other integral membrane or membrane-associated proteins or the integrity/solubility of crystallins.

Keywords

connexin; gap junction; transgenic mouse; cataract

1. Introduction

The lens is an avascular organ formed by an anterior epithelium and fiber cells that constitute the bulk of the organ. The plasma membranes of both epithelial and fiber cells contain specializations called gap junctions. Gap junctions contain clusters of intercellular channels formed by the co-axial alignment of two hemichannels or connexons. Each connexon is a hexameric assembly of subunit proteins called connexins (Cx). Co-expression of connexins may lead to the formation of heteromeric connexons (i.e., connexons made of more than one

* Corresponding author. Department of Pediatrics, Section of Hematology/Oncology, University of Chicago, 5841 S. Maryland Ave., MC 4060, Chicago, IL 60637, USA. Tel.: +1 773 702 6808; fax: +1 773 702 9881..

connexin). In the lens, epithelial cells predominantly express Cx43 (Beyer et al., 1989; Musil et al., 1990), and fiber cells mainly express Cx46 (Paul et al., 1991) and Cx50 (White et al., 1992; Church et al., 1995). Formation of heteromeric connexons in the lens has been demonstrated (Jiang and Goodenough, 1996; Berthoud et al., 2001).

Gap junction channels are permeable to ions and solutes of molecular mass up to 1000 Da. Because of their permeability properties, gap junction channels have been hypothesized to play a pivotal role in the maintenance of lens homeostasis and transparency (Goodenough, 1992). This hypothesis has been substantiated in recent years after generation of mice with targeted ablation of Cx46 (Gong et al., 1997) or Cx50 (White et al., 1998). These mice develop cataracts. Furthermore, genetic studies of some mouse strains or human pedigrees with inherited congenital cataracts have mapped the cataract trait to mutants of both Cx46 (Mackay et al., 1999) and Cx50 (Shiels et al., 1998; Steele et al., 1998).

The role of Cx50 in the lens is not limited to maintenance of lens transparency as mice lacking Cx50 not only develop cataracts but also exhibit microphakia (White et al., 1998). In contrast, Cx46-null mice have normal-sized lenses (Gong et al., 1997). Substitution of Cx46 for Cx50 restores lens transparency but does not prevent development of microphakia further supporting a specific role for Cx50 in lens growth (White, 2002).

Several children with partial duplications of the region of chromosome 1 containing the Cx50 locus exhibit multiple congenital anomalies, including cataracts (Chen et al., 1995; Finelli et al., 2001). This observation together with the data showing that Cx50 affects lens growth in mice raise the questions whether overexpression of Cx50 would lead to macrophakia or induce cataract formation or both. Thus, the present study was undertaken to determine the effects of overexpression of Cx50 protein in the lens.

2. Materials and methods

2.1. Chemicals

All chemicals were obtained from Sigma Chemical Co. (St. Louis, MO, USA) unless otherwise specified.

2.2. Antibodies

Rabbit polyclonal anti-human Cx50 antibodies have been previously described (Berthoud et al., 2003). Rabbit polyclonal anti-Cx46 antibodies were a generous gift from Dr. Thomas Steinberg (Washington University, St. Louis, MO). Mouse monoclonal and rabbit polyclonal anti-FLAG antibodies were obtained from Sigma. Mouse monoclonal anti-αA-, αB-, and β-crystallin antibodies were obtained from Stressgen Bioreagents (Victoria, British Columbia, Canada). Rabbit polyclonal anti-γ-crystallin antibodies were a generous gift from Dr. Samuel Zigler (NEI/NIH). Mouse monoclonal anti-N-cadherin antibody was obtained from BD Biosciences (San Jose, CA, USA). Rabbit polyclonal anti-aquaporin 0 (AQP0) antibodies and mouse monoclonal anti-ZO-1 antibody were obtained from Zymed Laboratories, Inc. (San Francisco, CA, USA). Cy2- or Cy3-conjugated goat anti-mouse IgG, Cy2- or Cy3-conjugated donkey anti-rabbit IgG and HRP-conjugated goat anti-rabbit IgG antibodies were obtained from Jackson ImmunoResearch (West Grove, PA, USA).

2.3. Generation of transgenic animals

Wild type Cx50 tagged with a FLAG (DYKDDDDK) epitope with an additional valine residue at its carboxyl terminus (FLAGV) was amplified from human genomic DNA by PCR (sense primer: 5′-attgtcgacgccgccaccatgggcgactggagtttcctgggg aacatcttg-3′, antisense primer: 5′-gcctctagaccttgtcgtcatcgtctttgt agtctacggttagatcgtctgacctggctcggctgct-3′). A DNA construct

containing nucleotides 1–464 of the βB1-crystallin promoter (accession number: M63906; Roth et al., 1991) followed by the sequence of wild type human Cx50-FLAGV was prepared. The DNA construct was microinjected into pronuclear stage CD-1 mouse embryos to obtain transgenic mice at the University of Chicago Transgenic and ES Cell-derived Mouse Facility. All studies were performed in non-transgenic and heterozygous transgenic animals, and whenever possible comparisons were made between non-transgenic and transgenic littermates. All animal studies were approved by the University of Chicago Institutional Animal Care and Use Committee and are in compliance with the EC Directive 86/609/EEC for animal experiments.

2.4. Electrophysiological measurements

The hCx50-FLAGV DNA construct was subcloned into the RNA expression vector, pSP64TII. The plasmid was linearized with EcoICR I, and capped RNA was synthesized using the mMessage mMachine SP6 in vitro transcription kit (Ambion, Austin, TX, USA) according to the manufacturer's instructions. The amount of RNA was quantified by measuring the absorbance at 260 nm.

Xenopus oocytes were prepared and tested as described previously (Ebihara et al., 1989). To measure the junctional conductance, cell pairs were studied using the dual two-micro-electrode technique (Spray et al., 1981). For simple measurements of gap junctional coupling, both cells of the pair were initially held at −40 mV and 5- to 10-mV steps were applied to one cell while holding the second cell at −40 mV. The junctional conductance (g_j) was calculated as I_j/V_j, where $V_j = V_{cell2} - V_{cell1}$. Data were acquired and analyzed using a personal computer running pCLAMP version 6.0.5 (Axon Instruments, Union City, CA, USA). Microelectrodes were filled with 3 M KCl (pH 7.4) and had resistances of 0.2–2 MΩ. The bath solution was modified Barth's solution. All of the experiments were performed on oocytes previously injected with antisense Cx38 oligonucleotides to ensure that the observed currents were caused by the expression of exogenous connexins (Ebihara, 1996).

2.5. Genotyping of transgenic mice

Incorporation of the full-length transgene construct into the mouse genome was assessed by PCR using genomic DNA isolated from tail biopsies as template and 2 sets of primers corresponding to sequences within the promoter region and the coding region of hCx50 (primer set 1, sense primer: 5′-ggtgggctctgggggtatatatgcc-3′, antisense primer: 5′-tagtgccttt gctgccgctgctct-3′) or within the coding region of hCx50 and the FLAGV epitope (primer set 2, sense primer: 5′-ctgccaag cctttcaatc-3′, antisense primer: 5′-ccttgtcgtcatcgtctt-3′). The expected sizes for the amplified bands are 834 and 411 bp for primer sets 1 and 2, respectively. Animals were considered transgenic only when the expected bands were amplified with both sets of primers. No amplification of bands was obtained using genomic DNA from non-transgenic littermates using either set of primers.

2.6. Gross anatomy

Darkfield photomicrographs were obtained with a Zeiss Stemi-2000C dissecting scope (Carl Zeiss, München, Germany). Wet lens weights from mice at different ages were obtained using an analytical microbalance. The results are expressed as the mean ± SEM. The differences in lens weights between transgenic and non-transgenic animals were analyzed for statistical significance using ANOVA test.

2.7. Optical quality analysis

Immediately following sacrifice via cervical dislocation, animals were enucleated and the lenses were removed in culture medium (M199, Invitrogen, Carlsbad, CA). A lens was

suspended by its equatorial rim on a beveled washer in a specially designed two-chambered glass and silicon rubber cell. Both surfaces of the lens were bathed in 25 ml of M199 with Earle's salts and 8% fetal bovine serum.

Average back vertex distance (BVD) and variability in BVD were quantified for the right lens from each animal in a Scantox™ In Vitro Assay System generously provided by Harvard Apparatus Inc. (Hollister, MA). This system consists of a collimated laser source that projects a 0.5 mm wide laser beam onto a mirror mounted on a carriage assembly at 45° (Sivak et al., 1994). The mirror reflects the laser beam directly up through the lens. The mirror carriage is controlled by a position motor connected to a drive screw which permits a series of parallel laser beams to be passed in defined steps across the lens. A digital camera captures the actual position and slope of the laser beam transmitted at each step. When all steps have been made, the captured data are used to calculate the average BVD, as well as the variability of the BVD. Eight laser beams were passed at equal increments, defined by dividing the equatorial diameter of the lens by the number of steps. In addition, the lens was rotated in 30° increments until the entire lens was scanned.

BVD was defined as measuring the laser beam from the rear surface of the lens to the focal point. Repeated measurements of BVD indicate instrument reproducibility within 0.32% of BVD. Changes in this distance with beam position are predominantly the result of longitudinal spherical aberration. Variability in BVD, defined as the average standard error of the means of the BVD of all laser scans, for each lens is an indication of the fine focusing capabilities. This parameter is affected by naturally occurring or pathologically-induced irregularities of the lens fibers.

Statistical analyses of differences between the BVD and variability in BVD were performed using a Mann–Whitney *t*-test for independent samples. A probability value of $p < 0.05$ was considered significant.

2.8. Light and electron microscopy analysis

Following laser scan analysis, lenses were fixed in 2.5% glutaraldehyde in 0.1 M cacodylic buffer pH 7.4 for 5 days at room temperature with daily changes of fixative. After overnight washing in 0.2 M sodium cacodylate buffer, the lenses were photographed under a Zeiss surgical dissecting microscope (New York, NY).

For light microscopy, lenses were post-fixed in 1% aqueous osmium tetroxide at 4 °C overnight, then washed in cacodylate buffer and dehydrated through a graded ethanol series to propylene oxide. Lenses were infiltrated and flat-embedded in epoxy resin. Sections (1 μm) were cut along the optic axis with a glass knife. Sections were mounted on glass slides and stained with a dilute mixture of methylene blue and azure II. Light micrographs were obtained using an Olympus Vanox AHBS3 microscope (Olympus America, Inc., Melville, NY) equipped with a 35 mm camera.

For scanning electron microscopy, lenses were split along the midline using a sharp blade and separated into sections. These specimens were post-fixed in 1% aqueous osmium tetroxide at 4 °C overnight, then washed in cacodylate buffer and dehydrated through a graded series of ethanols. After overnight dehydration in absolute ethanol, the alcohol was replaced by a graded series of Freon 113 in ethanol. The tissue was then dried on a Balzers CPD 020 (Balzers, Hudson, NH), secured onto aluminum stubs using silver paint, and sputter coated with gold under vacuum. The specimens were then examined on a JEOL JSM 35c SEM (JEOL USA, Peabody, MA) at 15 kV. Photomicrographs were obtained with a Polaroid camera system.

2.9. Immunofluorescence

Lenses for cryostat sections were fixed in 4% paraformaldehyde in phosphate buffered saline pH 7.4 (PBS) for 4 h at room temperature, transferred to 30% sucrose in PBS and left at 4 °C until they sank prior to sectioning at 12 μm. Cryostat sections were processed for immunofluorescence as previously described (Berthoud et al., 2004).

Confocal images were obtained using a Leica laser-scanning confocal microscope (Leica Microsystems, Exton, PA, USA) with laser settings of 500–535 nm for Cy2 and 600–615 nm for Cy3. Images were collected by sequential scanning using single laser-line excitation to eliminate bleeding from one channel into the other. Images were analyzed using Leica software. Composite figures were assembled using Adobe Photoshop 7.0 (Adobe Systems Inc., San Jose, CA, USA).

2.10. Immunoblotting

Lenses were dissected in PBS, homogenized in 10 mM Tris–HCl pH 7.5 containing 100 mM NaCl, 5 mM EDTA, 4 mM phenylmethylsulphonylfluoride, 10 μg/ml aprotinin, 10 μg/ml leupeptin, 10 μg/ml bestatin, 10 μg/ml pepstatin (Roche Diagnostics Corporation, Roche Applied Science, Indianapolis, IN, USA) in a glass–glass homogenizer, and then sonicated. Homogenates were either used immediately or stored at −80 °C until use.

Soluble and insoluble fractions were prepared according to Katar et al. (1993). They were also prepared following a minor modification of the method published by White et al. (1998). Lenses were dissected in PBS and homogenized in a solution containing 0.1 M NaCl, 0.1 M Na_2HPO_4, 10 mM ascorbic acid, 10 μg/ml leupeptin, 10 μg/ml pepstatin, 10 μg/ml aprotinin and 10 μg/ml bestatin using a glass–glass homogenizer. Homogenates were centrifuged at 14 000 g for 20 min at room temperature or at 4 °C. The supernatants (soluble fractions) were removed. The pellets were rinsed by resuspension in 0.1 M NaCl, 0.1 M Na_2HPO_4 and centrifuged at 14 000 g for 20 min at room temperature or at 4 °C (insoluble fractions). The insoluble fractions were extracted with 20 mM NaOH and centrifuged at 14 000 g for 20 min at room temperature or at 4 °C. Pellets were resuspended in a volume of SDS-loading buffer equal to that of the supernatant fraction. The soluble and insoluble fractions were stored at −80 °C. Similar results were obtained with any of the methods used.

Protein concentrations were determined using the BioRad Protein Assay (BioRad, Hercules, CA, USA) based on the Bradford dye-binding procedure (Bradford, 1976). For immunoblots of Cx50 and Cx46, 50 μg of protein from lens homogenates were resolved on 9% polyacrylamide gels containing SDS. For immunoblots of crystallins, 1 μg of protein from whole lens homogenates and corresponding proportions from the soluble and insoluble fractions were resolved on 12.5% polyacrylamide gels containing SDS. Then, proteins were transferred to Immobilon P membranes (Millipore, Bedford, MA) and membranes were subjected to immunoblotting as described (Berthoud et al., 2003). Relative levels of Cx50 proteins in transgenic and non-transgenic animals ($n \geq 3$) were determined by densitometry using an HP ScanJet 6100C/T scanner (Hewlett-Packard, Loveland, CO, USA) and Adobe Photoshop 7.0.

3. Results

3.1. Generation of βB1-hCx50-FLAGV transgenic mice

To determine the effects of overexpression of Cx50 in the lens, transgenic expression of Cx50 was specifically targeted to the lens by utilizing the chicken βB1-crystallin promoter which has been previously demonstrated to induce lens specific expression in transgenic mice (Duncan et al., 1995). Because the anti-Cx50 antibodies available could not distinguish

endogenous mouse Cx50 from transgenically expressed Cx50, an in-frame FLAG epitope tag was added at the carboxyl terminus of the coding region of Cx50. An additional valine was added following the FLAG tag to preserve the terminal amino acid residue of Cx50 (Fig. 1A). Thus, we refer to the coding region of this DNA construct as Cx50-FLAGV.

To test that the protein produced from the transgene construct was functional, *Xenopus* oocytes were injected with Cx50-FLAGV cRNA, and gap junctional conductance was determined in oocyte pairs by double whole-cell voltage-clamp. Expression of Cx50-FLAGV induced the formation of functional gap junction channels in *Xenopus* oocyte pairs with conductances that were significantly higher than background (Table 1). The junctional conductances induced by wild type hCx50 or hCx50-FLAGV cRNAs were not significantly different at either 6 or 24 h after pairing (Table 1, $p = 0.66$ and 0.49, respectively).

Initial screening of potential transgenic mouse pups by PCR identified several founders expressing the transgene that were designated 5, 14 and 63. An independent family (line) of transgenic mice was generated from each of these founders.

Expression of proteins derived from the transgene DNA in each line was assessed by immunoblotting (Fig. 1B, C). Several bands of 60–64 kDa (including a strong doublet that did not separate well on minigels) were detected in immunoblots of lens homogenates using anti-Cx50 antibodies. Corresponding bands that reacted with anti-FLAG antibodies were detected in samples from transgenic animals. No bands reacting with anti-FLAG antibodies were observed in non-transgenic mice. The anti-Cx50 immunoreactive bands were consistently more intense in lens homogenates prepared from transgenic animals than those prepared from non-transgenic littermates. However, the magnitude of the increase was variable in lens homogenates prepared from line 14 mice (Fig. 1B, C, lanes 5–8). Densitometric analysis revealed that levels of immunoreactive Cx50 in transgenic lenses were on average 4.0 and 13.6 times those of non-transgenic animals for lines 5 and 63, respectively. No attempt at quantifying the increase in levels of Cx50 was made for line 14, because these lenses were quite fragile; they ruptured and broke into pieces upon dissection. No cleaved forms of Cx50 or degradation products were detected in samples from non-transgenic or transgenic animals even though the anti-Cx50 antibodies used can recognize cleaved forms of Cx50.

3.2. Lens size, structure, and ultrastructure

Visual inspection of the mouse eyes revealed lens opacities in all transgenic animals (Fig. 2A, B). Cataracts were observed as early as postnatal day 1 (the first age studied). The severity of the phenotype varied among the different lines with line 14 showing the most severe cataracts.

Lack of expression of Cx50 in the lens has previously been associated with decreased lens growth (Sellito et al., 2004). The lenses of Cx50 transgenic mice appeared smaller than those of non-transgenic mice (compare Fig. 2A and B). To assess the effects of hCx50 overexpression upon lens growth, lenses from transgenic and non-transgenic littermates from each line were dissected at different postnatal ages and weighed. Lenses of transgenic mice from line 14 weighed significantly less than those of their non-transgenic littermates from postnatal day 7 onwards; transgenic lenses from lines 5 and 63 were significantly lighter from postnatal days 10 and 15 onwards (Fig. 3; also compare Fig. 2A and B and Fig. 4A and B). The lack of a significant difference in lens weight between non-transgenic and transgenic mice during early postnatal life may reflect the limitations of weighing these small lenses.

The lens abnormalities associated with these cataracts were analyzed in histological preparations. Disorganization of the overall lens structure was observed in transgenic mice, but the severity of the alterations varied among the different lines (Fig. 4). Compared to lenses from non-transgenic animals, lenses from transgenic animals showed posterior displacement

of the differentiating zone, irregularities of fiber cell size and shape, and persistence of nuclei in lens fibers (Fig. 4, compare A with B and C). The abnormal cell shape was seen not only at the equator (Fig. 4, compare E with F and G), but also in cross-sections (Fig. 4, compare H with I and J which correspond to the anterior region). Note the development of normal regions of radial cell columns in the wild type as well as in line 63 (Fig. 4H, I). Lens fiber necrosis (zones of liquefaction) was common (Fig. 4B, C, F and J). In several lenses, pseudostratification of the epithelium was observed. While lenses from non-transgenic animals showed a few areas of apparent cell fusion and pentagonal-shaped cells (Fig. 4H, arrows), transgenic animals had more abnormally shaped cells and areas of cell fusion (Fig. 4I, arrows). Lenses from transgenic animals of line 14 showed the most dramatic alterations; in most cases, extrusion of a considerable proportion of the lenticular mass was observed (Fig. 4D). Disruption of the capsule and loss of the majority of the lens mass probably explain the variability in the levels of Cx50 in this line as determined by immunoblotting. Therefore, lenses from this line were subjected to limited analysis.

Analysis of mouse lenses by scanning electron microscopy revealed disturbances in cell fiber organization (Fig. 5A–D). Lens fibers from non-transgenic animals had the characteristic S-shape structure expected for these cells (Fig. 5A). In transgenic lenses, the S-shaped structure of fiber cells could still be distinguished at low magnification (Fig. 5B), but the shape and width of fiber cells were not as uniform as in the wild type lens (Fig. 5, compare panels C and D); bulging areas along single lens fibers were observed (Fig. 5D). Differences in fiber cell width might reflect osmotic changes as swelling has been observed in osmotic cataracts; bulges may reflect localized osmotic changes. Alternatively, when strings of interdigitations of fiber cells bifurcate, they may represent fusions or abnormally shaped cells with membrane distortions.

3.3. Optical quality of the lens

The optical quality of lenses from transgenic and non-transgenic animals was analyzed by laser scanning, a technique that involves measurement of the deflection of a laser beam impacting the lens at different angles. Lenses from non-transgenic animals exhibited normal optical quality. In contrast, the presence of a large central cataract precluded assessment and/or quantification of lens optical quality in most lenses from transgenic animals. Even in the few cases in which analysis of lenses from transgenic animals was possible, the optical quality ranged from poor to very poor. The back focal length was increased in transgenic animals (1.476 ± 0.128 mm compared to 1.098 ± 0.081 mm in non-transgenic animals).

3.4. Localization of lens connexins

The distribution of Cx50 was studied by immunofluorescence using rabbit polyclonal anti-Cx50 antibodies and a mouse monoclonal anti-N-cadherin antibody (to label the plasma membrane of fiber cells). Well restricted domains of anti-Cx50 and anti-N-cadherin immunoreactivities were observed at the plasma membrane of fiber cells in lens sections from non-transgenic animals (Fig. 6A–C, arrows); as expected, no intracellular anti-Cx50 immunostaining was observed in these sections. In contrast, lens sections from transgenic animals showed immunoreactivity to anti-Cx50 antibodies at fiber cell appositional membranes (Fig. 6D–F, arrows) and in cytoplasmic vesicle-like structures (Fig. 6D–F, arrowheads and Fig. 6G–I). Deconvolved confocal images showed that these cytoplasmic Cx50-containing structures had a ring-like appearance, suggesting that the protein was localized to the vesicle membrane (data not shown). Some overlap between N-cadherin and Cx50 immunoreactivities was detected in these vesicles (Fig. 6I). Three-dimensional reconstruction of a *z*-series of confocal images from a vesicle suggested a close proximity of Cx50 vesicles to the fiber cell plasma membrane (see Supplementary material). Interestingly, after three-dimensional reconstruction, the N-cadherin staining seemed to trail from the fiber

cell plasma membrane to the overlapping areas, suggesting continuity between the vesicle and the plasma membrane. Because the anti-Cx50 antibodies used also recognized endogenous mouse Cx50, the distribution of the protein encoded by the transgene was also assessed by double labeling immunofluorescence using rabbit polyclonal anti-FLAG antibodies and a mouse monoclonal anti-N-cadherin antibody. Similar to the distribution observed with anti-Cx50 antibodies, immunolabeling was observed at appositional membranes and cytoplasmic vesicles in lens sections from transgenic animals (Fig. 6J–L, arrows and arrowheads, respectively). The anti-FLAG immunoreactive vesicles showed little overlap with N-cadherin except when the vesicular structures were in close proximity with the plasma membrane (Fig. 6J–L, thin arrows). No anti-FLAG immunoreactivity was observed in lens sections from non-transgenic littermates (data not shown).

To test whether transgenic expression of Cx50 affected the levels or distribution of Cx46, lens samples from transgenic animals were studied by immunoblotting and double label immunofluorescence. No major differences in the levels of Cx46 were detected between transgenic and non-transgenic mouse lenses by immunoblotting (Fig. 7A). Immunofluorescence of lens sections from non-transgenic animals showed discrete domains within the plasma membranes of fiber cells immunolabeled with anti-Cx46 antibodies and anti-N-cadherin antibodies; no overlap between the two signals was detected in cross-sections (Fig. 7B, D, F). Sections of transgenic lenses were immunostained using rabbit polyclonal anti-Cx46 antibodies and a mouse monoclonal anti-FLAG antibody. Similar to the distribution of Cx46 in the lenses from non-transgenic mice, immunoreactivity to anti-Cx46 antibodies localized at appositional membranes in fiber cells. While anti-Cx46 immunoreactivity co-localized with anti-FLAG immunoreactivity at the plasma membrane (Fig. 7C, E, G, arrows), little if any anti-Cx46 immunoreactivity was associated with the anti-FLAG immunoreactive intracellular vesicles (Fig. 7C, E, G, arrowheads). In cases when the anti-FLAG immunopositive vesicles localized close to the plasma membrane, the immunoreactivities appeared to overlap along the vesicular rim (Fig. 7C, E, G, thin arrows) suggesting that Cx46 in gap junction plaques was in close proximity to a preformed Cx50-containing vesicle or to a vesicle in the process of budding off from the plasma membrane; no vesicles appeared completely yellow.

3.5. Localization of AQP0

Connexin45.6, the chicken ortholog of Cx50, shows a developmentally regulated interaction with AQP0 (Yu and Jiang, 2004). To test the possibility that increased levels of Cx50 altered the distribution of AQP0, we performed double label immunofluorescence on lens sections using anti-AQP0 antibodies in combination with anti-Cx50 or anti-FLAG antibodies. In lenses from non-transgenic animals, anti-AQP0 and anti-Cx50 immunoreactivities localized to the plasma membrane; no major overlap between the two signals was observed except when the plane of the section was not perpendicular to the long axis of the fibers (Fig. 8A–C). In lenses from transgenic animals, anti-AQP0 immunoreactivity localized to the plasma membrane of fiber cells; its distribution revealed the striking changes in lens fiber cell shape resulting from overexpression of Cx50. Only a minor amount of anti-AQP0 immunoreactivity overlapped with the intracellular anti-FLAG immunopositive staining; this overlap was observed when vesicles were located in close proximity to the plasma membrane (Fig. 8D–F, arrowheads).

3.6. Effect of overexpression of Cx50 on ZO-1

ZO-1, a member of the membrane-associated guanylate kinase family, is expressed in fiber cells where it localizes predominantly along the narrow sides of fiber cells in the outer cortex and along the broad sides in the middle and deep cortex, where it co-localizes with Cx50 (Nielsen et al., 2003). To test whether overexpression of Cx50 affected the distribution of ZO-1, we performed double labeling immunofluorescence on lens sections from non-transgenic and transgenic animals using anti-Cx50 and anti-ZO-1 antibodies. The distribution of ZO-1 in non-

transgenic lenses was similar to that previously described for wild type mice (Fig. 9A, B). In transgenic lenses, ZO-1 was also mainly present on the narrow sides of fiber cells in the outer cortex (Fig. 9C–E). Deeper in the cortex, the overall anti-ZO-1 immunostaining was not as regular as that observed in non-transgenic animals reflecting the variations in size and shape of lens fibers in transgenic lenses (Fig. 9, compare panels A and B with C and F). Nevertheless, co-localization of ZO-1 and Cx50 immunoreactivities at the plasma membrane was frequently observed (Fig. 9F–H, arrows). Most cytoplasmic Cx50-containing vesicles showed little anti-ZO-1 immunoreactivity. Occasional partial staining of a vesicle for ZO-1 corresponded to the superposition of Cx50 immunostaining of vesicles in close proximity to the plasma membrane with that of ZO-1 at the plasma membrane (Fig. 9F–H, thin arrows).

3.7. Effect of overexpression of Cx50 on lens crystallins

Many cataracts including those of the Cx46- and Cx50-null mice (Gong et al., 1997; White, 2002) have been associated with decreased solubility of crystallins. Cataracts in Cx46-null mouse are also associated with proteolysis of γ-crystallin (Gong et al., 1997). To test whether crystallin solubility or integrity was altered in the transgenic Cx50 mice, we performed immunoblots on lens homogenates and on soluble and insoluble fractions prepared from transgenic and non-transgenic animals using anti-αA-, αB-, β- or γ-crystallin antibodies. No major differences were observed in the levels of crystallins in total homogenates (Fig. 10, lanes 1 and 2) or in the lens soluble fractions (Fig. 10, lanes 3 and 4) between transgenic and non-transgenic animals. No αA-, αB- or β-crystallin were detected in the insoluble fractions (Fig. 10A–C, lanes 5 and 6). A small but similar amount of γ-crystallin was detected in the insoluble fractions prepared from non-transgenic and transgenic animals (Fig. 10D, lanes 5 and 6). No major differences in the levels of γ-crystallin were detected in the insoluble fractions obtained after NaOH extraction (data not shown).

4. Discussion

We have demonstrated that mice expressing a functional, epitopetagged Cx50 transgene protein have small lenses with cataracts. The observed abnormalities likely resulted from the expression of the transgene, not its insertional position, since all three transgenic lines showed a similar phenotype.

The decreased size of the lenses in mice expressing the transgene Cx50 supports a role for Cx50 in lens growth. A relationship between Cx50 and lens growth was previously suggested based on the observation that lenses from Cx50-null mice are significantly smaller than lenses from wild type mice from postnatal day 3 onwards (Sellito et al., 2004). In contrast, mice with a single copy of Cx50 (heterozygous null mutation) have normal sized lenses (White et al., 1998). Thus, taking together these results with our findings, a direct relationship between levels of Cx50 and lens size is not supported, rather it appears that any drastic alterations in Cx50 expression (either absence or overexpression) decrease lens size.

Our results suggest that Cx50 may participate in the differentiation of lens cells, because the lenses from the transgenic animals exhibited features of abnormal differentiation including a posteriorly displaced bow region and persistence of nuclei deep into the lens. These results are rather surprising, because overexpression of the Cx50 chicken ortholog, Cx45.6, in cultured chicken lens cells accelerates lentoid formation (Gu et al., 2003). Extrapolating from these results, lenses from the Cx50 transgenic mice might have been expected to undergo early differentiation of epithelial cells and to have an anteriorly displaced bow region. However, our studies showed the opposite findings. These discrepancies might reflect differences between the in vivo and in vitro systems or between mouse and chicken lenses.

The lenses of several transgenic mouse models exhibit abnormalities that suggest impairment of epithelial to fiber cell differentiation. Similar to the transgenic Cx50 lenses, several of these models show impairment of the denucleation process (Capetanaki et al., 1989; Dunia et al., 1990; Perez-Castro et al., 1993; Martin et al., 1995; Cammarata et al., 1999; West-Mays et al., 2002; Duncan et al., 2004). However, while the transgenic Cx50 mice showed a posterior displacement of the bow region, the bow region was displaced anteriorly in mice with high expression of Na^+/myoinositol co-transporter (Cammarata et al., 1999) or ectopic expression of the AP-2α transcription factor (West-Mays et al., 2002). Some transgenic models also show impaired elongation of the fiber cells leading to flattening of the lens surface or production of a lumen (Capetanaki et al., 1989; Perez-Castro et al., 1993; Duncan et al., 2004), features that were not found in the transgenic Cx50 mouse lenses. Fiber cells in the Cx50 transgenic mouse lenses exhibited irregular cell shapes, disordered packing, bulges along single fiber cells and abundant Cx50-immunoreactive intracellular vesicles. Some of these abnormalities have also been observed in other transgenic mouse models (Dunia et al., 1990; Perez-Castro et al., 1993; Duncan et al., 2004). Because fiber cells showed abnormalities but elongation did not seem to be directly affected, the smaller lenses in the transgenic Cx50 mice may result from delayed differentiation of epithelial cells and a decreased number of cells.

Several other mouse lines have been generated with transgenic expression of different proteins in the lens. Although many of these animals exhibit lens abnormalities, not all of them develop cataracts. For example, transgenic expression of desmin (Dunia et al., 1990) or wild type myocillin (Zillig et al., 2005) in the lens does not lead to cataract development nor does expression of low levels of major histocompatibility complex class I (Martin et al., 1995) or Na^+/myoinositol co-transporter (Cammarata et al., 1999). These results imply that there are specific effects of the transgenic Cx50 protein that lead to cataract development.

Several lines of evidence suggest that the mechanisms leading to cataract formation in mice overexpressing Cx50 differ from those in the Cx46- and Cx50-null mice. The connexin-null animals have reductions in intercellular communication due to the absence of those connexins (Gong et al., 1998; Baldo et al., 2001). In contrast, it is unlikely that the phenotype of the Cx50 transgenics can be explained by a loss of gap junctional communication, since hCx50-FLAGV induced junctional conductances in paired *Xenopus* oocytes at levels that were not significantly different from wild type hCx50. Rather, these animals may have lens gap junctions with altered permeability and/or regulatory properties which are dominated by those of the Cx50 channels, since Cx50 constitutes an increased fraction of the fiber cell connexins in these animals. Moreover, the biochemical abnormalities differ between the connexin-null and transgenic mice; while crystallin integrity/solubility is decreased in the cataracts of both connexin-null mice, the mice overexpressing Cx50 showed no crystallin proteolysis or changes in crystallin solubility. In addition, unlike the cataracts observed in the Cx46- or Cx50-null mice which are evident at 2–3 weeks or 1 week of postnatal age, respectively, the lens opacities in transgenic Cx50 mice were already present at postnatal day 1, the earliest age analyzed. The presence of nuclear cataracts by this age is probably due to expression of the Cx50 transgene driven by the βB1 promoter which is active in both primary and secondary fiber cells.

Cataract formation in the Cx50 transgenic mice might also result from the effects of Cx50 overexpression on interacting proteins. The formation of abundant intracellular vesicles containing Cx50 could lead to trapping/accumulation of other proteins (e.g., Cx46, AQP0 or ZO-1) and consequent deficiencies at their proper sites.

Cx46 was a likely candidate to be affected by overexpression of Cx50, since association of Cx46 and Cx50 in the lens has been demonstrated by co-precipitation experiments (Jiang and Goodenough, 1996). However, Cx46 was readily detected at appositional membranes, and it was not present in the intracellular vesicles. In the Cx50 transgenic mice, levels of Cx46 were

comparable to those detected in non-transgenic animals. Similarly, in Cx50-null mice and in chicken lens cultures overexpressing Cx45.6 (the chicken ortholog of Cx50), levels of Cx46 (or its chicken ortholog Cx56) are not affected (White et al., 1998; Gu et al., 2003).

Another likely candidate that could be affected was AQP0, since AQP0 and chicken Cx45.6 interact during early embryonic development of the chicken lens (Yu and Jiang, 2004). However, overexpression of Cx50 only affected the distribution of AQP0 to a minor extent, as some of its immunoreactivity was found in the Cx50-containing intracellular vesicles. No associated decrease in anti-AQP0 immunoreactivity at the plasma membrane was detectable. Moreover, even if present, such a modest AQP0 reduction could not account for the cataracts, since heterozygous mice with a 50% AQP0 reduction do not develop cataracts until 24 months of age (Shiels et al., 2001).

Another possible interacting protein that might have been affected was ZO-1, since Cx50 and other connexins have been shown to interact with it (Toyofuku et al., 1998; Kausalya et al., 2001; Laing et al., 2001; Nielsen et al., 2003). However, overexpression of Cx50 did not interfere with the preferential localization of ZO-1 to the narrow and broad sides of fiber cells in the outer and deeper cortex, respectively. It was possible that the epitope tag at the carboxyl terminus of the trans-gene protein may have interfered with the interaction between ZO-1 and Cx50, since the association of ZO-1 with mouse Cx50 requires its most carboxyl terminal amino acid (isoleucine) (Nielsen et al., 2003), but the presence of a carboxyl terminal FLAG tag in Cx43 (a connexin known to interact with ZO-1) does not interfere with the association between ZO-1 and that connexin (Toyofuku et al., 1998). The exact role of the Cx50-ZO-1 interaction in the lens has not been determined, but multiple dynamic roles have been suggested (Nielsen et al., 2003) based on the roles ascribed to the interaction of ZO-1 with Cx43 and Cx45. The interaction of ZO-1 with those connexins has been implicated in transport of Cx43 to the plasma membrane (Wu et al., 2003), redistribution of connexin from lipid rafts to gap junctional plaques which confers Triton-X-100 insolubility (Laing et al., 2005, 2006), assembly of gap junctional plaques (Toyofuku et al., 1998; Singh et al., 2005), regulation of gap junction function (Toyofuku et al., 1998; Laing et al., 2005) by scaffolding of proteins involved in signaling pathways (Giepmans and Moolenar, 1998; Kausalya et al., 2001), and gap junction endocytosis and turnover (Barker et al., 2002; Segretain et al., 2004). Whether the interaction of Cx50 with ZO-1 underlies any of these roles remains to be determined. Indeed, it is unclear that any major interactions between Cx50 and ZO-1 take place in the differentiating fibers, where Cx50-containing gap junction assembly occurs, since Cx50 and ZO-1 are located on opposite sides of these fiber cells. Moreover, mouse Cx50 lacking the carboxyl terminal isoleucine forms gap junctional plaques even though it does not bind to the ZO-1 PDZ2 domain (Nielsen et al., 2003). Deeper in the lens cortex, where Cx50 and ZO-1 co-localize, interactions may have some yet undefined role.

Alternatively, overexpression of Cx50 might have globally affected membrane proteins by overwhelming the cellular synthetic machinery and the secretory pathway. However, this hypothesis seems unlikely, because AQP0, N-cadherin and Cx46 all reached the plasma membrane quite efficiently. Lastly, we cannot rule out the possibility that other unidentified proteins interact with Cx50 and that this interaction may have been affected by the presence of the carboxyl terminal tag.

Accumulation of some normal proteins in the lens has been associated with human cataracts (e.g., hereditary hyperferritinemia and Alzheimer's disease) (Brooks et al., 2002; Goldstein et al., 2003). Moreover, cataracts have been observed in transgenic mice expressing a secretion-defective mutant myocillin that accumulates in vesicles corresponding to dilated rough endoplasmic reticulum cisternae in the bow region (Zillig et al., 2005). However, in the Cx50 transgenic mouse, the double label immunofluorescence studies suggest that the vesicles form

by internalization of the plasma membrane and not because of a protein secretion abnormality; the electrophysiological data suggest normal targeting of the transgenic protein to the plasma membrane.

Thus, the most likely factor contributing to the lens abnormalities in the transgenic mice is the Cx50-containing cytoplasmic vesicles. The vesicles would themselves scatter light and impair lens transparency. Their persistence in differentiating fibers would eventually lead to cellular damage and necrosis. Further studies of the Cx50 transgenic mouse model will help elucidate the biochemical mechanisms underlying cataract formation.

Supplementary Material

Refer to Web version on PubMed Central for supplementary material.

Acknowledgements

This work was supported by NIH grants EY-08368 (to ECB), EY-06642 (to JRK), and EY-10589 (to LE), a grant from the Children's Research Foundation (to VMB), and the Bernice Meltzer Pediatric Cancer Research Fund. The authors are indebted to Dr. Linda Degenstein from the University of Chicago Transgenic and ES Cell-derived Mouse Facility for the generation of the transgenic mice and her advice. The authors would also like to acknowledge Dr. Vytas Bindokas from the Confocal Facility of the University of Chicago for his expert advice and Drs. Emily Kistner and Theodore Karrison of the Biostatistics Consulting Laboratory within the Department of Health Studies, supported by the University of Chicago Cancer Research Center, for their assistance with the statistical analysis of the data.

References

Baldo GJ, Gong X, Martinez-Wittinghan FJ, Kumar NM, Gilula NB, Mathias RT. Gap junctional coupling in lenses from α_8 connexin knockout mice. J Gen Physiol 2001;118:447–456. [PubMed: 11696604]

Barker RJ, Price RL, Gourdie RG. Increased association of ZO-1 with connexin43 during remodeling of cardiac gap junctions. Circ Res 2002;90:317–324. [PubMed: 11861421]

Berthoud VM, Minogue PJ, Guo J, Williamson EK, Xu X, Ebihara L, Beyer EC. Loss of function and impaired degradation of a cataract-associated mutant Cx50. Eur J Cell Biol 2003;82:209–221. [PubMed: 12800976]

Berthoud VM, Montegna EA, Atal N, Aithal NH, Brink PR, Beyer EC. Heteromeric connexons formed by the lens connexins, connexin43 and connexin56. Eur J Cell Biol 2001;80:11–19. [PubMed: 11211930]

Berthoud VM, Singh R, Minogue PJ, Ragsdale CW, Beyer EC. Highly restricted pattern of connexin36 expression in chick somite development. Anat Embryol 2004;209:11–18. [PubMed: 15455226]

Beyer EC, Kistler J, Paul DL, Goodenough DA. Antisera directed against connexin43 peptides react with a 43-kD protein localized to gap junctions in myocardium and other tissues. J Cell Biol 1989;108:595–605. [PubMed: 2537319]

Bradford MM. A rapid and sensitive method for the quantitation of microgram quantities of protein using the principle of protein–dye binding. Anal Biochem 1976;72:248–254. [PubMed: 942051]

Brooks DG, Manova-Todorova K, Farmer J, Lobmayr L, Wilson RB, Eagle RC Jr, St Pierre TG, Stambolian D. Ferritin crystal cataracts in hereditary hyperferritinemia cataract syndrome. Investig Ophthalmol Vis Sci 2002;43:1121–1126. [PubMed: 11923255]

Cammarata PR, Zhou C, Chen G, Singh I, Reeves RE, Kuszak JR, Robinson ML. A transgenic animal model of osmotic cataract. Part 1: over-expression of bovine Na^+/myoinositol cotransporter in lens fibers. Investig Ophthalmol Vis Sci 1999;40:1727–1737. [PubMed: 10393042]

Capetanaki Y, Smith S, Heath JP. Overexpression of the vimentin gene in transgenic mice inhibits normal lens cell differentiation. J Cell Biol 1989;109:1653–1664. [PubMed: 2793935]

Chen H, Tuck-Muller CM, Batista DA, Wertelecki W. Identification of supernumerary ring chromosome 1 mosaicism using fluorescence in situ hybridization. Am J Med Genet 1995;56:219–233. [PubMed: 7625449]

Church RL, Wang JH, Steele E. The human lens intrinsic membrane protein MP70 (Cx50) gene –clonal analysis and chromosome mapping. Curr Eye Res 1995;14:215–221. [PubMed: 7796604]

Duncan MK, Roth HJ, Thompson M, Kantorow M, Piatigorsky J. Chicken βB1 crystallin: gene sequence and evidence for functional conservation of promoter activity between chicken and mouse. Biochim Biophys Acta 1995;1261:68–76. [PubMed: 7893762]

Duncan MK, Xie L, David LL, Robinson ML, Taube JR, Cui W, Reneker LW. Ectopic Pax6 expression disturbs lens fiber cell differentiation. Investig Ophthalmol Vis Sci 2004;45:3589–3598. [PubMed: 15452066]

Dunia I, Pieper F, Manenti S, van de Kemp A, Devilliers G, Benedetti EL, Bloemendal H. Plasma membrane–cytoskeleton damage in eye lenses of transgenic mice expressing desmin. Eur J Cell Biol 1990;53:59–74. [PubMed: 2076709]

Ebihara L. *Xenopus* connexin38 forms hemi-gap-junctional channels in the nonjunctionalplasmamembrane of *Xenopus* oocytes. Biophys J 1996;71:742–748. [PubMed: 8842212]

Ebihara L, Beyer EC, Swenson KI, Paul DL, Goodenough DA. Cloning and expression of a *Xenopus* embryonic gap junction protein. Science 1989;243:1194–1195. [PubMed: 2466337]

Finelli P, Cavalli P, Giardino D, Gottardi G, Natacci F, Savasta S, Larissa L. FISH characterization of a supernumerary r(1)(::cen → q22::q22 → sq21::) chromosome associated with multiple anomalies and bilateral cataracts. Am J Med Genet 2001;104:157–164. [PubMed: 11746048]

Giepmans BNG, Moolenar WH. The gap junction protein connexin43 interacts with the second PDZ domain of the zona occludens-1 protein. Curr Biol 1998;8:931–934. [PubMed: 9707407]

Goldstein LE, Muffat JA, Cherny RA, Moir RD, Ericsson MH, Huang X, Mavros C, Coccia JA, Faget KY, Fitch KA, Masters CL, Tanzi RE, Chylack LT Jr, Bush AI. Cytosolic β-amyloid deposition and supranuclear cataracts in lenses from people with Alzheimer's disease. Lancet 2003;361:1258–1265. [PubMed: 12699953]

Gong X, Baldo GJ, Kumar NM, Gilula NB, Mathias RT. Gap junctional coupling in lenses lacking α_3 connexin. Proc Natl Acad Sci USA 1998;95:15303–15308. [PubMed: 9860964]

Gong X, Li E, Klier G, Huang Q, Wu Y, Lei H, Kumar NM, Horwitz J, Gilula NB. Disruption of α3 connexin gene leads to proteolysis and cataractogenesis in mice. Cell 1997;91:833–843. [PubMed: 9413992]

Goodenough DA. The crystalline lens. A system networked by gap junctional intercellular communication. Semin Cell Biol 1992;3:49–58. [PubMed: 1320431]

Gu S, Yu XS, Yin X, Jiang JX. Stimulation of lens cell differentiation by gap junction protein connexin 45.6. Investig Ophthalmol Vis Sci 2003;44:2103–2111. [PubMed: 12714649]

Jiang JX, Goodenough DA. Heteromeric connexons in lens gap junction channels. Proc Natl Acad Sci USA 1996;93:1287–1291. [PubMed: 8577756]

Katar M, Alcala J, Maisel H. NCAM of the mammalian lens. Curr Eye Res 1993;12:191–196. [PubMed: 8449028]

Kausalya PJ, Reichert M, Hunziker W. Connexin45 directly binds to ZO-1 and localizes to the tight junction region in epithelial MDCK cells. FEBS Lett 2001;505:92–96. [PubMed: 11557048]

Laing JG, Chou BC, Steinberg TH. ZO-1 alters the plasma membrane localization and function of Cx43 in osteoblastic cells. J Cell Sci 2005;118:2167–2176. [PubMed: 15855237]

Laing JG, Koval M, Steinberg TH. Association with ZO-1 correlates with plasma membrane partitioning in truncated connexin45 mutants. J Membr Biol 2006;207:45–53. [PubMed: 16463142]

Laing JG, Manley-Markowski RN, Koval M, Civitelli R, Steinberg TH. Connexin45 interacts with zonula occludens-1 and connexin43 in osteoblastic cells. J Biol Chem 2001;276:23051–23055. [PubMed: 11313345]

Mackay D, Ionides A, Kibar Z, Rouleau G, Berry V, Moore A, Shiels A, Bhattacharya S. Connexin 46 mutations in autosomal dominant congenital cataract. Am J Hum Genet 1999;64:1357–1364. [PubMed: 10205266]

Martin WD, Egan RM, Stevens JL, Woodward JG. Lens-specific expression of a major histocompatibility complex class I molecule disrupts normal lens development and induces cataracts in transgenic mice. Investig Ophthalmol Vis Sci 1995;36:1144–1154. [PubMed: 7537260]

Musil LS, Beyer EC, Goodenough DA. Expression of the gap junction protein connexin43 in embryonic chick lens: molecular cloning, ultrastructural localization, and post-translational phosphorylation. J Membr Biol 1990;116:163–175. [PubMed: 2166164]

Nielsen PA, Baruch A, Shestopalov VI, Giepmans BNG, Dunia I, Benedetti EL, Kumar NM. Lens connexins α3Cx46 and α8Cx50 interact with zonula occludens protein-1 (ZO-1). Mol Biol Cell 2003;14:2470–2481. [PubMed: 12808044]

Paul DL, Ebihara L, Takemoto LJ, Swenson KI, Goodenough DA. Connexin46, a novel lens gap junction protein, induces voltage-gated currents in nonjunctional plasma membrane of *Xenopus* oocytes. J Cell Biol 1991;115:1077–1089. [PubMed: 1659572]

Perez-Castro AV, Tran VT, Nguyen-Huu MC. Defective lens fiber differentiation and pancreatic tumorigenesis caused by ectopic expression of the cellular retinoic acid-binding protein I. Development 1993;119:363–375. [PubMed: 8287793]

Roth HJ, Das GC, Piatigorsky J. Chicken βB1-crystallin gene expression: presence of conserved functional Polyomavirus enhancer-like and octamer binding-like promoter elements found in non-lens genes. Mol Cell Biol 1991;11:1488–1499. [PubMed: 1996106]

Segretain D, Fiorini C, Decrouy X, Defamie N, Prat JR, Pointis G. A proposed role for ZO-1 in targeting connexin 43 gap junctions to the endocytic pathway. Biochimie 2004;86:241–244. [PubMed: 15194225]

Sellito C, Li L, White TW. Connexin50 is essential for normal post-natal lens cell proliferation. Investig Ophthalmol Vis Sci 2004;45:3196–3202. [PubMed: 15326140]

Shiels A, Bassnett S, Varadaraj K, Mathias R, Al-Ghoul K, Kuszak J, Donoviel D, Lilleberg S, Friedrich G, Zambrowicz B. Optical dysfunction of the crystalline lens in aquaporin-0-deficient mice. Physiol Genomics 2001;7:179–186. [PubMed: 11773604]

Shiels A, Mackay D, Ionides A, Berry V, Moore A, Bhattacharya S. A missense mutation in the human connexin50 gene (GJA8) underlies autosomal dominant ‘‘zonular pulverulent’’ cataract, on chromosome 1q. Am J Hum Genet 1998;62:526–532. [PubMed: 9497259]

Singh D, Solan JL, Taffet SM, Javier R, Lampe PD. Connexin 43 interacts with zona occludens-1 and -2 proteins in a cell cycle stage-specific manner. J Biol Chem 2005;280:30416–30421. [PubMed: 15980428]

Sivak JG, Herbert KL, Peterson KL, Kuszak JR. The interrelationship of lens anatomy and optical quality. I Non-primate lenses Exp Eye Res 1994;59:505–520.

Spray DC, Harris AL, Bennett MVL. Equilibrium properties of a voltage-dependent junctional conductance. J Gen Physiol 1981;77:77–93. [PubMed: 6259274]

Steele EC Jr, Lyon MF, Favor J, Guillot PV, Boyd Y, Church RL. A mutation in the connexin 50 (Cx50) gene is a candidate for the No2 mouse cataract. Curr Eye Res 1998;17:883–889. [PubMed: 9746435]

Toyofuku T, Yabuki M, Otsu K, Kuzuya T, Hori M, Tada M. Direct association of the gap junction protein connexin-43 with ZO-1 in cardiac myocytes. J Biol Chem 1998;273:12725–12731. [PubMed: 9582296]

West-Mays JA, Coyle BM, Piatigorsky J, Papagiotas S, Libby D. Ectopic expression of AP-2α transcription factor in the lens disrupts fiber cell differentiation. Dev Biol 2002;245:13–27. [PubMed: 11969252]

White TW. Unique and redundant connexin contributions to lens development. Science 2002;295:319–320. [PubMed: 11786642]

White TW, Bruzzone R, Goodenough DA, Paul DL. Mouse Cx50, a functional member of the connexin family of gap junction proteins, is the lens fiber protein MP70. Mol Biol Cell 1992;3:711–720. [PubMed: 1325220]

White TW, Goodenough DA, Paul DL. Targeted ablation of connexin50 in mice results in microphthalmia and zonular pulverulent cataracts. J Cell Biol 1998;143:815–825. [PubMed: 9813099]

Wu JC, Tsai RY, Chung TH. Role of catenins in the development of gap junctions in rat cardiomyocytes. J Cell Biochem 2003;88:823–835. [PubMed: 12577316]

Yu XS, Jiang JX. Interaction of major intrinsic protein (aquaporin-0) with fiber connexins in lens development. J Cell Sci 2004;117:871–880. [PubMed: 14762116]

Zillig M, Wurm A, Grehn FJ, Russell P, Tamm ER. Overexpression and properties of wild-type and Tyr437His mutated myocillin in the eyes of transgenic mice. Investig Ophthalmol Vis Sci 2005;46:223–234. [PubMed: 15623777]

Abbreviations

AQP0
: aquaporin 0

Cx
: connexin

PBS
: phosphate buffered saline, pH 7.4

Appendix A. Supplementary information

Supplementary data associated with this article can be found, in the online version, at doi: 10.1016/j.exer.2006.11.004.

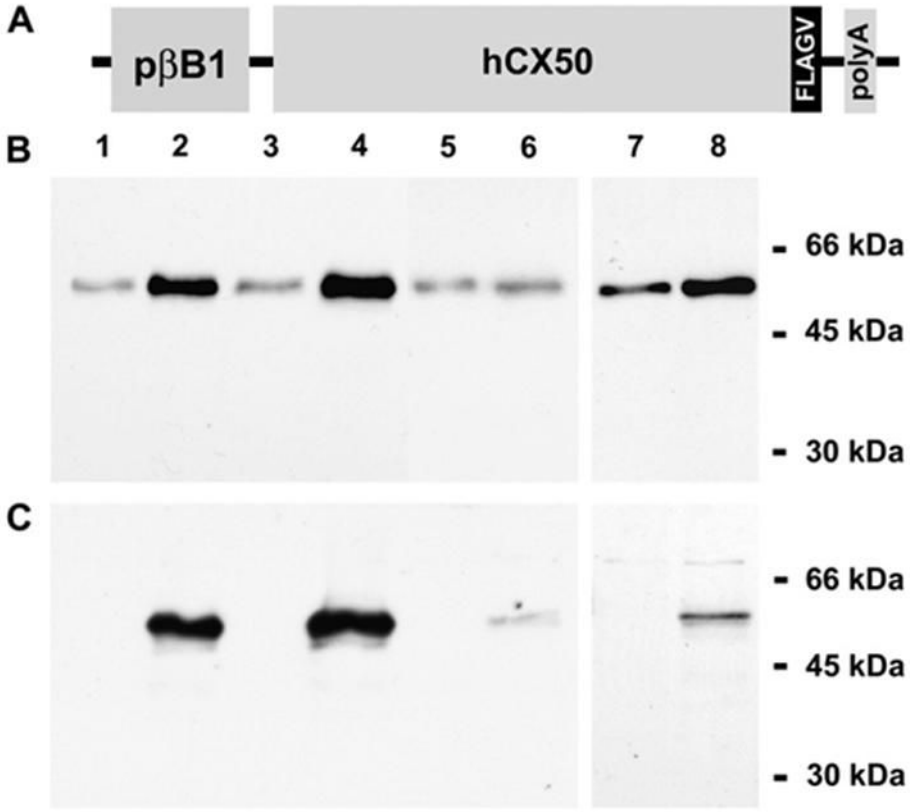

Fig. 1.

Generation of Cx50 transgenic mice and evaluation of transgenic protein expression. (A) Diagram of the transgene construct containing the βB1-crystallin promoter (pβB1), the coding region of human Cx50 (hCx50), an inframe epitope tag (FLAGV) at the carboxyl terminus of Cx50 and a polyA signal (polyA). (B, C) Whole lens homogenates from 2-month-old non-transgenic (lanes 1, 3, 5 and 7) and transgenic (lanes 2, 4, 6 and 8) litter-mates from lines 5 (lanes 1 and 2), 63 (lanes 3 and 4) and 14 (lanes 5–8) were analyzed by immunoblotting in duplicate blots using rabbit polyclonal anti-Cx50 (B) or mouse monoclonal anti-FLAG (C) antibodies. The positions to which the molecular mass standards migrated are indicated on the right. An increased intensity of the Cx50 immunoreactive bands was detected in samples from transgenic animals of each line as expected. Note the absence of a cleaved form of Cx50 in either non-transgenic or transgenic lens homogenates.

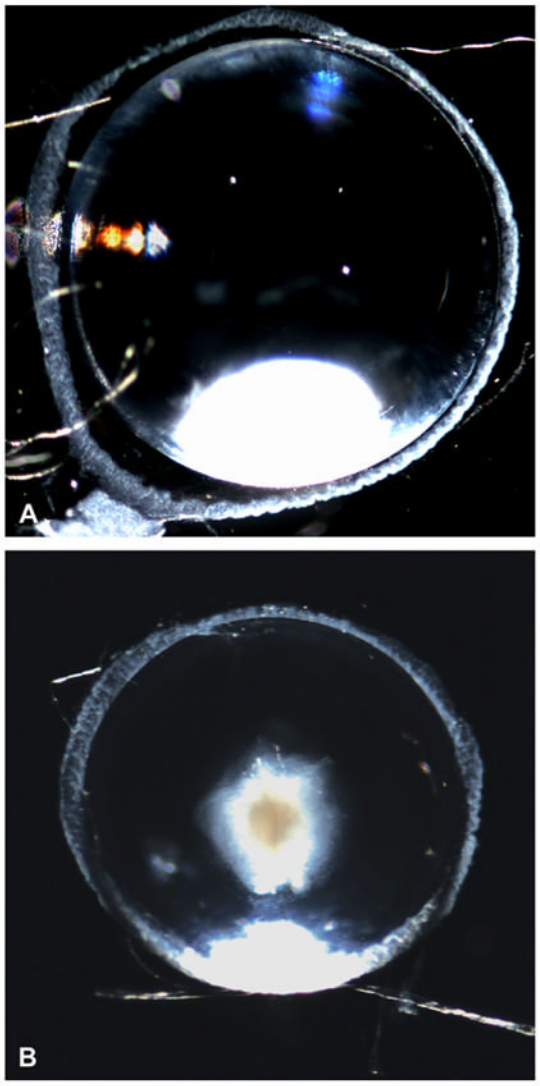

Fig. 2.
Differences in appearance of lenses from normal and transgenic mice. (A, B) Darkfield photomicrographs of lenses from a 1-month-old non-transgenic (A) and a transgenic (B) littermate from line 63. Note the presence of a central cataract and the decreased size of the transgenic lens.

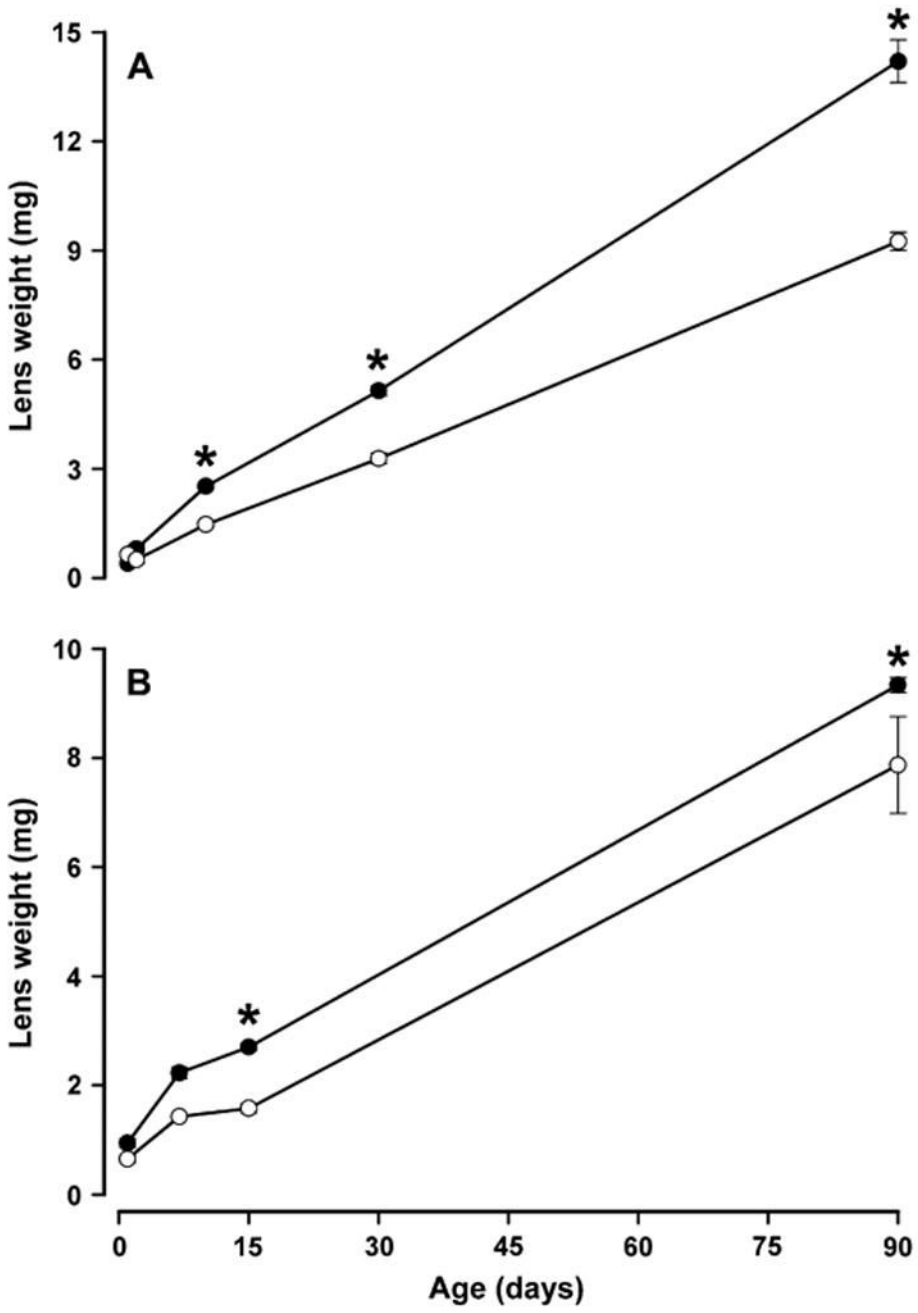

Fig. 3.

Effect of expression of transgenic Cx50 on lens weight. Graphs show the weight of lenses from lines 5 (A) and 63 (B) at different postnatal ages for non-transgenic (-●-) and transgenic (-○-) animals. The data are presented as mean ± SEM. Asterisks indicate significant differences ($p < 0.05$) between the lens weight of non-transgenic and transgenic animals of the same age and line analyzed by ANOVA test.

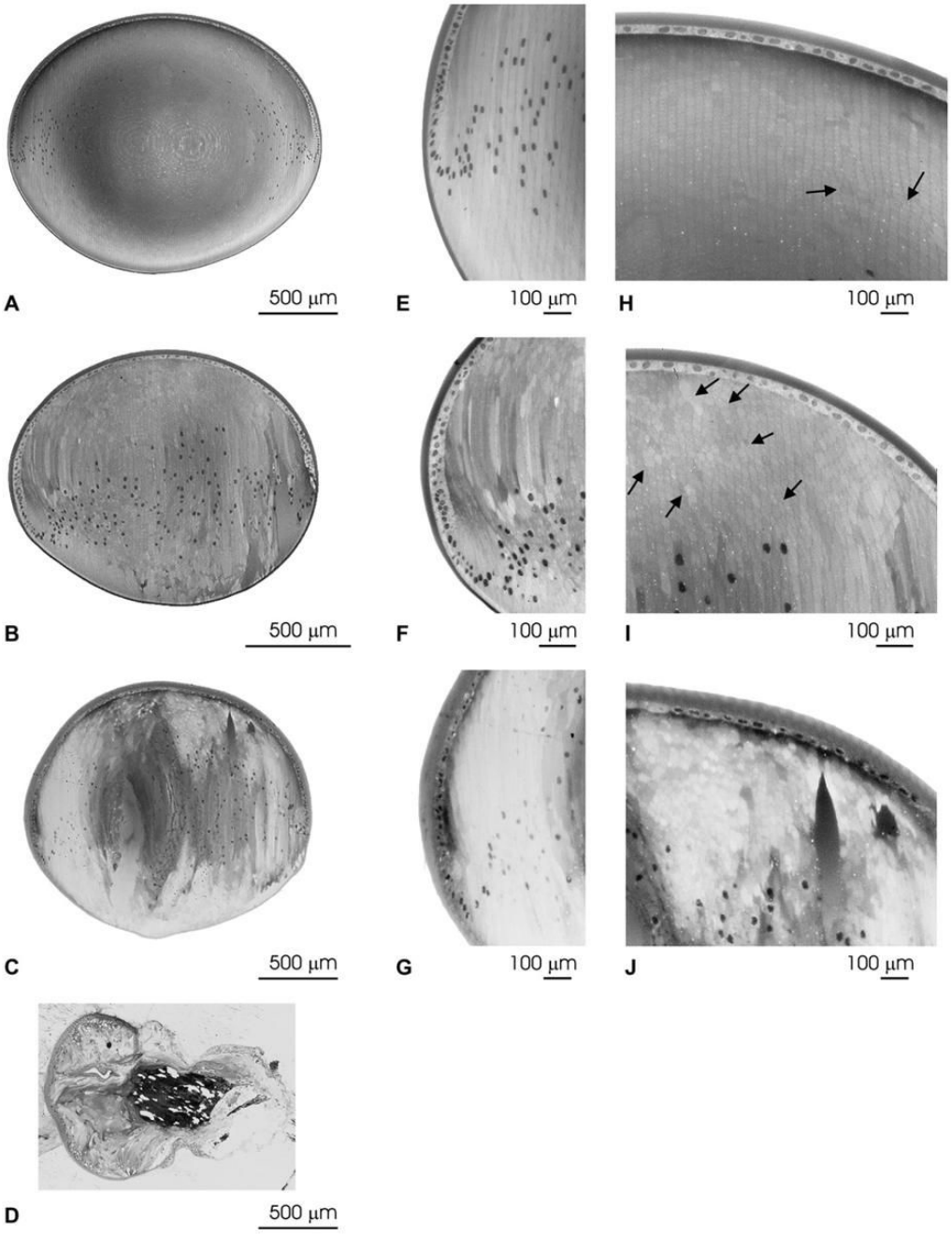

Fig. 4.

Histological analysis of the lenses from transgenic animals. Light micrographs of the whole lens (A–D), the equatorial region (E–G), and the anterior region (H–J) of non-transgenic (A, E, H), and transgenic mice from line 63 (B, F, I), line 5 (C, G, J), and line 14 (D). Disorganization of the overall lens structure with areas of liquefaction can be seen in lens sections from transgenic mice. Panel D shows an example of a lens from line 14 in which extrusion occurred as was the case in more than 90% of the lenses from this line. Arrows indicate areas of cell fusion with pentagonal cells among the normal hexagonal lens fiber cells. Magnification bars are indicated in each panel.

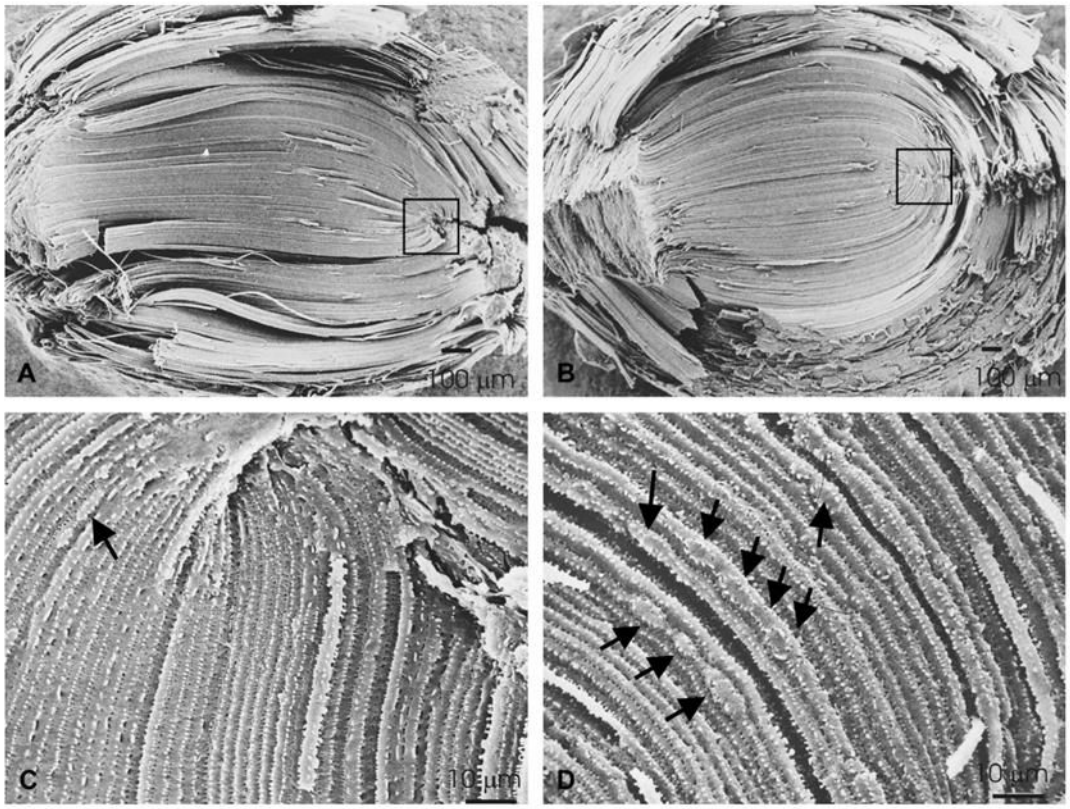

Fig. 5.

Structural and ultrastructural analysis of lenses overexpressing Cx50. Scanning electron micrographs of non-transgenic (A, C) and transgenic (B, D), line 63 mouse lenses. (A and B) At low magnification, the S-shaped structure of fibers can be seen in both types of lenses. (C and D) At higher magnification, it is clear that the shape and the width of fiber cells in the transgenic lenses are not as uniform as in the non-transgenic lenses and areas with bulges along single fiber cells are evident (arrows). Magnification bars are indicated in each panel.

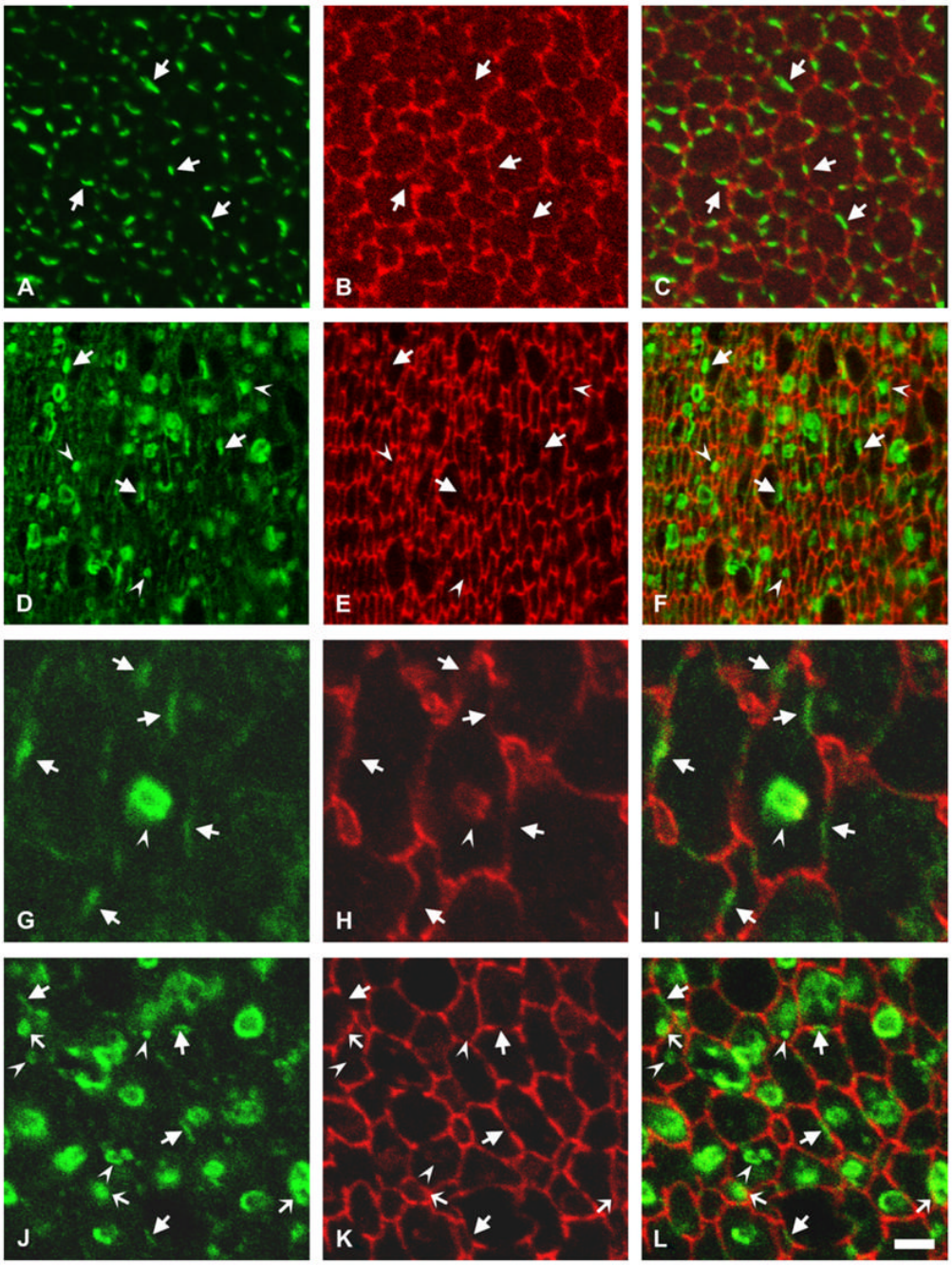

Fig. 6.

Distribution of the transgene Cx50 protein. (A–C) Photomicrographs show immunolocalization of Cx50 in cross-sections of postnatal day 10 lenses from non-transgenic mice from line 5 after double labeling immunofluorescence using rabbit polyclonal anti-Cx50 antibodies (A) and a mouse monoclonal anti-N-cadherin antibody (B). (D–F) Photomicrographs show immunolocalization of Cx50 in cross-sections of postnatal day 10 lenses from transgenic mice from line 5 after double labeling immunofluorescence using rabbit polyclonal anti-Cx50 antibodies (D) and a mouse monoclonal anti-N-cadherin antibody (E). (G–I) A vesicle-like structure observed at higher magnification after double labeling immunofluorescence with rabbit polyclonal anti-Cx50 antibodies (G) and a mouse monoclonal

anti-N-cadherin antibody (H). (J–L) Photomicrographs show immunolocalization of the transgene Cx50 in cross-sections of postnatal day 10 lenses from transgenic mice from line 5 after double labeling immunofluorescence using rabbit polyclonal anti-FLAG antibodies (J) and a mouse monoclonal anti-N-cadherin antibody (K). The immunostaining for Cx50 or the FLAG epitope tag is shown in green and that for N-cadherin is shown in red. The merged images are shown in C, F, I and L. Sections from transgenic mice show abundant immunoreactivity to anti-Cx50 or -FLAG antibodies localized intracellularly (F, L). Irregularities in cell diameter and organization of lens fiber cells are evidenced by the anti-N-cadherin staining (E, K). Anti-Cx50 or anti-FLAG immunoreactivity at the plasma membrane of fiber cells is indicated by arrows; intracellular staining is indicated by arrowheads. Overlap between the anti-FLAG immunoreactivity in vesicles and anti-N-cadherin immunoreactivity at the plasma membrane is indicated by thin arrows in panels J–L. The brightness of the cytoplasmic vesicles in the transgenic lenses precluded the use of the laser beam at the same intensity for image acquisition of lens sections from transgenic and non-transgenic animals; thus, while Cx50 and FLAG immunoreactivities were readily detected along fiber cell membranes in transgenic animals, this is not always apparent in the images shown (compare panels Awith D and J). Bar: 8 μm for A–F, 2 μm for G–I and 4 μm for J–L.

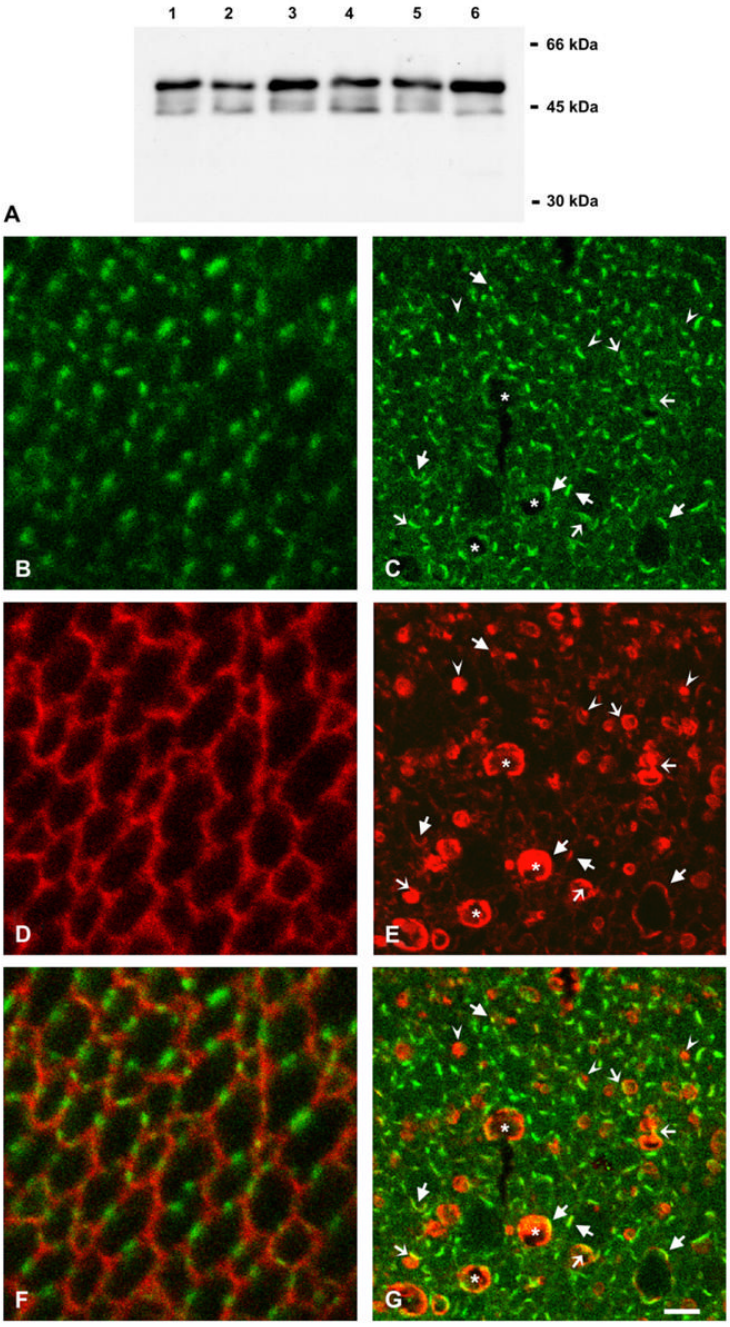

Fig. 7.

Effects of the Cx50 transgene on levels and distribution of Cx46. (A) Immunoblot of whole lens homogenates from 2-month-old non-transgenic (lanes 1, 3, 5) and transgenic (lanes 2, 4, 6) mice from lines 5 (lanes 1 and 2), 63 (lanes 3 and 4) and 14 (lanes 5 and 6) using rabbit polyclonal anti-Cx46 antibodies. (B–G) Confocal images of lens sections from 10-day-old non-transgenic (B, D, F) and transgenic (C, E, G) mice from line 5 after double labeling immunofluorescence using rabbit polyclonal anti-Cx46 antibodies (B, C) and a mouse monoclonal anti-N-cadherin (D) or anti-FLAG (E) antibody. Immunoreactivity to anti-Cx46 antibodies is shown in green and that to anti-N-cadherin or anti-FLAG antibody is shown in red. The superposition of the signals is shown in F, G. Note the co-localization of Cx46 and

epitope tag immunoreactivities at the plasma membrane of fiber cells (arrows). The intracellular vesicles that are immunopositive for the epitope tag antibody show little or no overlap with the anti-Cx46 immunoreactivity (arrowheads) except when they localize close to the plasma membrane (thin arrows). Some cells with abnormal shape or very large vesicles showing extensive anti-FLAG immunostaining (asterisks) have overlap with anti-Cx46 immunoreactivity only along their perimeter. Bar: 8 μm.

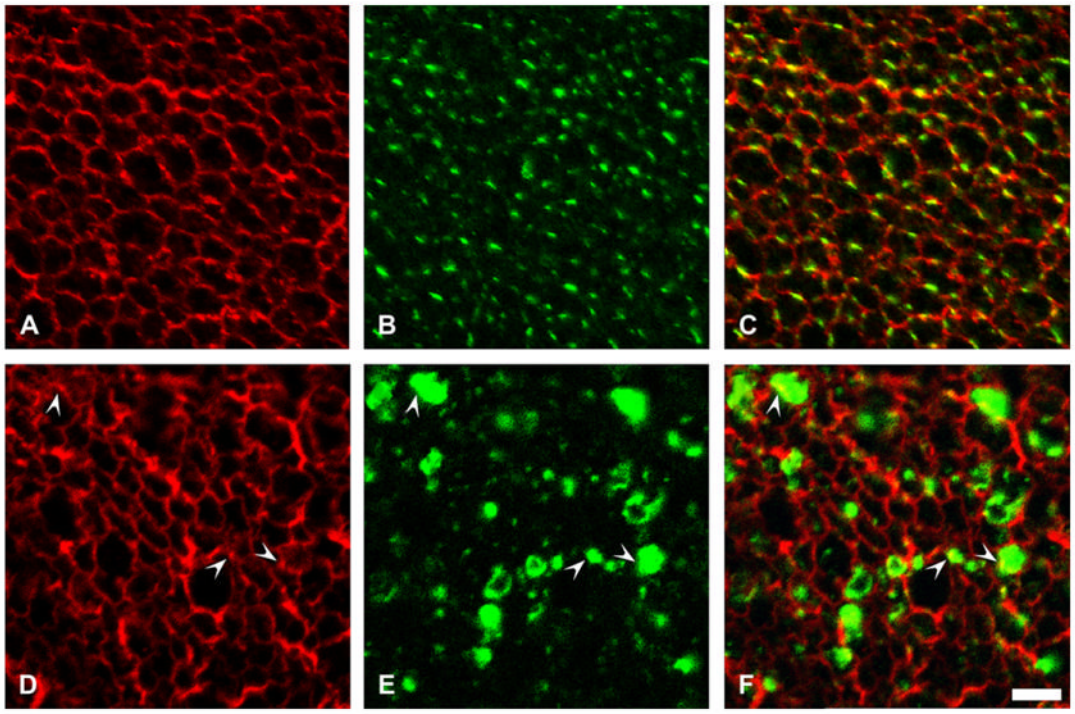

Fig. 8.

Effect of overexpression of Cx50 on AQP0 distribution. (A–C) Confocal images show the distribution of AQP0 in a lens section from a 10-day-old non-transgenic mouse from line 5 after double label immunofluorescence using rabbit polyclonal anti-AQP0 antibodies (A) and a mouse monoclonal anti-Cx50 antibody (B). (D–F) Confocal images show the distribution of AQP0 in a lens section from a 10-day-old transgenic mouse from line 5 after double label immunofluorescence using rabbit polyclonal anti-AQP0 antibodies (D) and a mouse monoclonal anti-FLAG antibody (E). Immunoreactivity to anti-AQP0 antibodies is shown in red and that to anti-Cx50 or anti-FLAG antibody is shown in green. The superposition of the two signals is shown in C and F. Overlap between the anti-Cx50 and anti-MIP immunoreactivities was observed in the non-transgenic animals when the plane of the section was not completely perpendicular to the long axis of the lens fibers. In the transgenic lenses, a minor overlap between immunoreactivities to anti-AQP0 and anti-FLAG antibodies is observed (arrowheads). Bar: 8 μm.

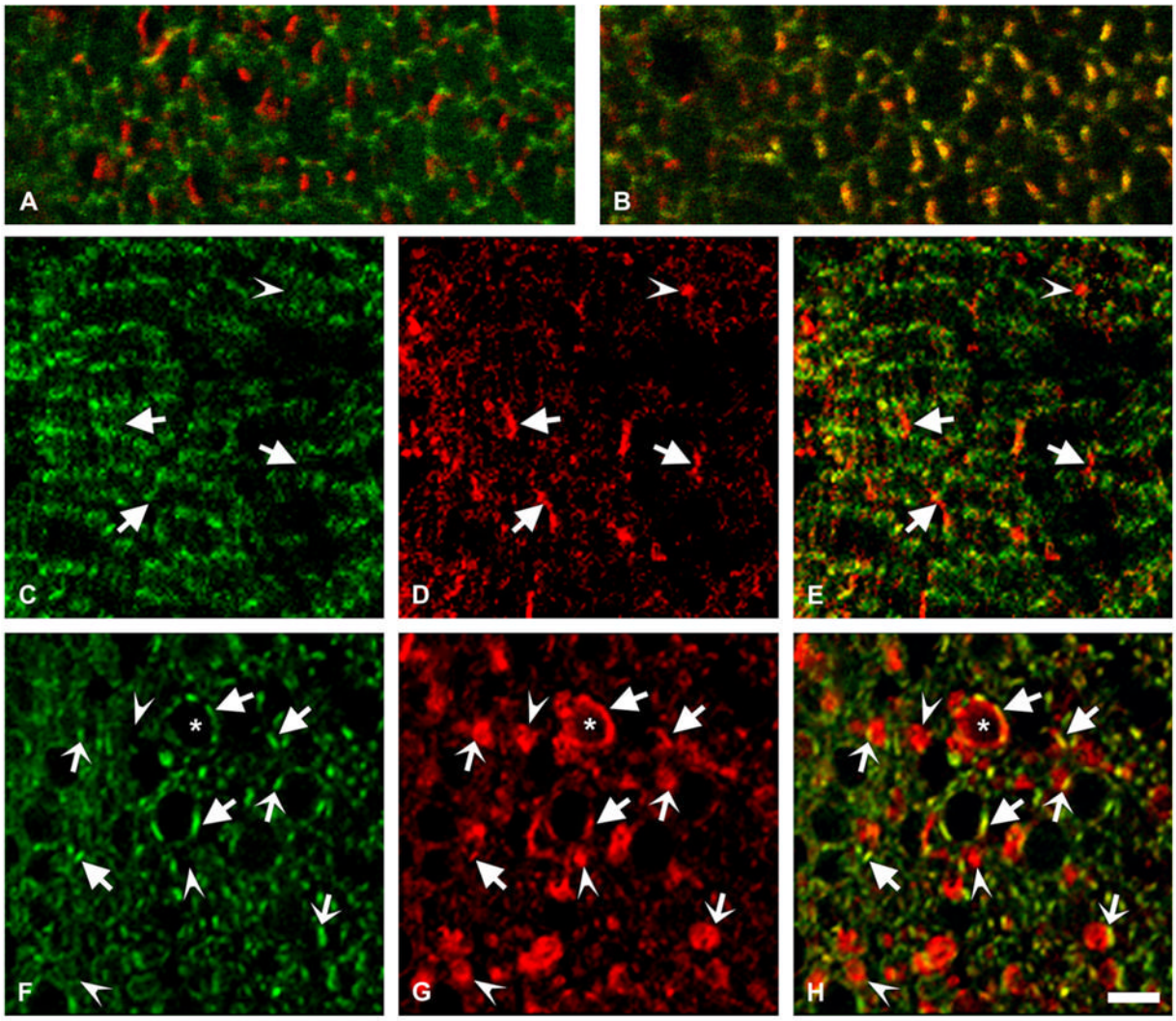

Fig. 9.

Effect of Cx50 overpexpression on ZO-1 distribution. (A, B) Confocal images show a superposition of immunoreactivities to a mouse monoclonal anti-ZO-1 and rabbit polyclonal anti-Cx50 antibodies in lens sections from a 10-day-old non-transgenic mouse from line 5 in the outer (A) and deeper (B) cortex. Immunostaining for ZO-1 is shown in green and that for Cx50 is shown in red; the overlap of the two signals appears yellow. (C–H) Confocal images obtained from the outer cortex (C–E) and deeper cortex (F–H) of lens sections from a 10-day-old mouse from line 5 after double labeling immunofluorescence using a mouse monoclonal anti-ZO-1 and rabbit polyclonal anti-Cx50 antibodies. Immunoreactivity to anti-ZO-1 antibodies is shown in green (C, F) and that to anti-Cx50 antibodies is shown in red (D, G). Overlap of the two signals appears yellow (E, H). Immunoreactivity to anti-Cx50 antibodies at the plasma membrane (arrows) showed little overlap with ZO-1 in the outer cortex and significant overlap in the deeper cortex. Cx50-containing vesicles that show little or no overlap with ZO-1 are indicated by arrowheads. Overlap in vesicles that are in close proximity to the plasma membrane is seen as a yellow line (thin arrows). The membrane of a cell with an amorphous non-hexagonal shape shows an extended region of immunoreactivity to anti-Cx50 antibodies (asterisk) suggesting presence of Cx50 around most of the cell perimeter. Bar: 5 μm for A and B, 8 μm for C–H.

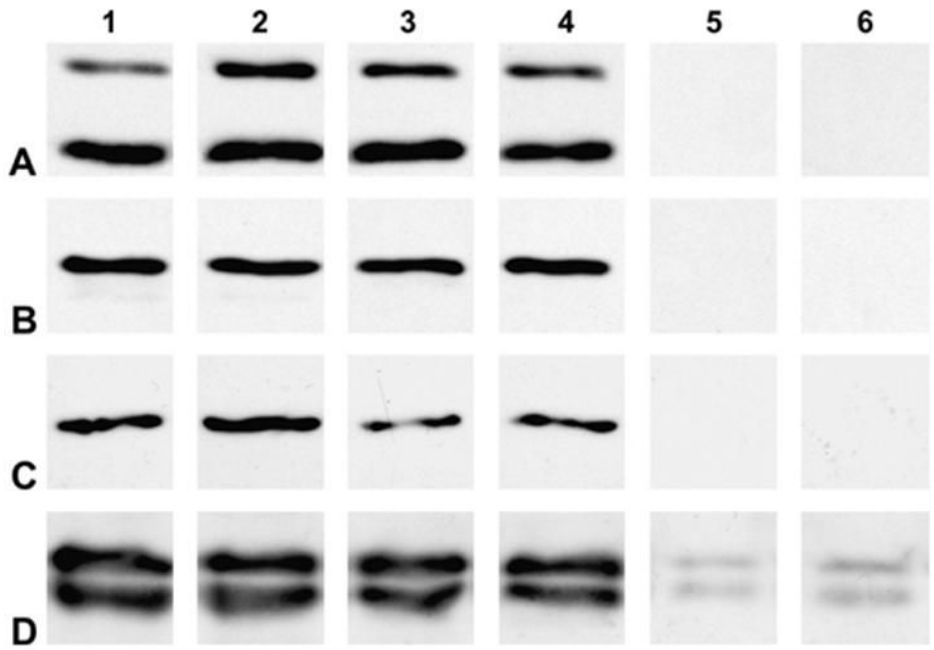

Fig. 10.

Effects of expression of the Cx50 transgene on solubility of crystallins. Immunoblots of total homogenates (lanes 1 and 2), soluble fractions (lanes 3 and 4) and insoluble fractions (lanes 5 and 6) prepared from non-transgenic (lanes 1, 3 and 5) and transgenic (lanes 2, 4 and 6) mouse lenses from line 5 using anti-αA-, anti-αB-, anti-β- or anti-γ-crystallin (A–D, respectively) antibodies. Samples from 6-month-old and 4-month-old mice were used for immunoblots of αA- and αB-crystallin and β- and γ-crystallin, respectively. No major differences in the levels of the studied crystallins or their distribution between soluble and insoluble fractions were detected between non-transgenic and transgenic lenses.

Table 1

Time after pairing (h)	Injected RNA	Gap junctional conductance (μS) Mean ± SEM	*n*
6	None	0.144 ± 0.022	5
	Wild type hCx50	1.135 ± 0.117	7
	hCx50-FLAGV	1.258 ± 0.251	7
24	None	0.189 ± 0.026	6
	Wild type hCx50	9.493 ± 6.648	9
	hCx50-FLAGV	4.591 ± 2.757	10